On the synthesis, characterization and magnetic properties of two new phases discovered in the PbO-Fe2O3-P2O5 system

Hassan El Hafid, Matias Velázquez, Olivier Pérez, Abdelaziz El Jazouli, Alain Pautrat, Rodolphe Decourt, Emmanuel Véron, Oudomsack Viraphong, Claude Delmas

On the synthesis, characterization and magnetic properties of two new phases discovered in the $PbO–Fe_2O_3–P_2O_5$ system

Hassan El Hafid [a], Matias Velázquez [a,*], Olivier Pérez [b], Abdelaziz El Jazouli [c], Alain Pautrat [b], Rodolphe Decourt [a], Emmanuel Véron [d], Oudomsack Viraphong [a], Claude Delmas [a]

[a] CNRS, Université de Bordeaux, ICMCB, 87 avenue du Dr. A. Schweitzer, 33608 Pessac cedex, France
[b] Laboratoire de Cristallographie et Sciences des Matériaux, UMR 6508 CNRS/Université de Caen, 6 Boulevard du Maréchal Juin, 14050 Caen cedex 04, France
[c] Laboratoire de Chimie des Matériaux Solides, URAC 17, Université Hassan II Mohammedia, Faculté des Sciences Ben M'Sik, Casablanca, Morocco
[d] Conditions Extrêmes et Matériaux: Haute Température et Irradiation, CEMHTI-CNRS UPR 3079, 1D avenue de la Recherche Scientifique, 45071 Orléans cedex 2, France

A B S T R A C T

The $PbFe_3O(PO_4)_3$ powder compound was studied by means of X-ray diffraction (XRD) from 300 to 6 K, electron-probe microanalysis (EPMA) coupled with wavelength dispersion spectroscopy (WDS), calorimetric (DSC and specific heat) and magnetic properties measurements. Magnetization, magnetic susceptibility and specific heat measurements carried out on $PbFe_3O(PO_4)_3$ powders firmly establish a series of three ferromagnetic (FM)-like second order phase transitions spanned over the 32–8 K temperature range. Discrepancies between magnetization and specific heat data obtained in $PbFe_3O(PO_4)_3$ powders and single crystals are highlighted. A first extraction of the critical exponents (β,γ,δ) was performed by ac magnetic susceptibility in both $PbFe_3O(PO_4)_3$ powders and single crystals and the values were found to be consistent with mean-field theory. Further exploration of the $PbO–Fe_2O_3–P_2O_5$ system led to the discovery of a new langbeinite phase, $Pb_{1.5}Fe_2(PO_4)_3$, the crystal structure of which was solved by room temperature single crystal XRD ($P2_13$, $Z=4$, $a=9.7831(2)$ Å). This phase does not undergo any structural phase transition down to 6 K nor any kind of long range ordering down to 2 K.

1. Introduction

A fast riffle through the ICSD [1] database reveals that 27% of the 2102 purely inorganic phosphate compounds are non-centrosymmetric, which is less than the 35% of borate counterparts but more than the average 15% of inorganic crystals. Ninety-two percent of the 576 non-centrosymmetric phosphates are 3*d* transition metal ones. A selective summary of optical and magneto-optical most salient features in several phosphates has been given recently in Ref. [2], to which we should add the discovery in 1970 of the cooperative luminescence mechanism of Yb^{3+}-pairs in the $YbPO_4$ crystals [3]. Among them, Fe^{3+} and Mn^{2+} phosphates are particularly interesting to investigate for several reasons. As long as the ratio of the crystal field parameter over the B Racah parameter (Dq/B) remains lower than ~3, the electronic ground state of their $3d^5$ configuration is an orbital singlet ($L=0$) and a spin sextet ($S=5/2$) which, broadly speaking, leads to isotropic magnetic exchange (strong or moderate AFM superexchange couplings at 180° or 90° predicted by the GKA rules and absence of spin–orbit interaction), and is very likely to be handled within the convenient framework of classical spins approximation. In addition, they do not undergo static Jahn–Teller effect whatever the point symmetry. This ground state spin sextet is unique among the 246 excited states arising from this configuration (containing ~39% of spin quartets), which forbids *d–d* intraconfigurational transitions, either intraatomic or between first neighbors. All in all, these quantum characteristics generally simplify the understanding of the magnetic and optical properties of these compounds. Amorphous $FePO_4$ thin films were prepared and their use as optical waveguide material was investigated because of their refractive index ≈1.6–1.7 in the visible spectral range [4]. On the other hand, magnetic 1D compounds have been shown to exhibit striking magnetooptical effects such as the giant enhancement of spin-forbidden optical transitions by an exchange mechanism due to the spreading of antiferromagnetic correlations at room temperature, in the absence of long range order [5]. Magnetization slow decays could lead in the future to magnetic information storage at the building units level of the crystal structure. Recently, $PbFe_3O(PO_4)_3$ single crystals were synthesized by El Hafid et al. [2] by a combination of Bridgman and high-temperature solution methods and found to exhibit a sequence of three FM-like magnetization divergencies at 31.8, 23.4 and 10.0 K.

In this work, we decided to explore further the synthesis, growth and magnetic properties of the $PbFe_3O(PO_4)_3$ compound.

* Corresponding author. Fax: +33 5 40 00 27 61.
E-mail address: matias.velazquez@icmcb-bordeaux.cnrs.fr (M. Velázquez).

In addition to establishing the heretofore unknown magnetic properties of the $PbFe_3O(PO_4)_3$ powder phase, we discovered a new phase in the $PbO–Fe_2O_3–P_2O_5$ pseudo-ternary system, namely $Pb_{1.5}Fe_2(PO_4)_3$, the crystal structure of which was solved by single crystal X-ray diffraction (XRD). Its specific heat was also measured as a function of temperature.

2. Material, methods and results

2.1. Synthesis, crystal growth and powder X-ray characterization

$PbFe_3O(PO_4)_3$ was prepared via a co-precipitation route. $Pb(NO_3)_2$, $Fe(NO_3)_3 \cdot 9H_2O$ (R. P. Normapur Prolabo, 98.0%) and $(NH_4)_2HPO_4$ (Prolabo Rhône-Poulenc, 97–100%) were used as reactants. These reactants were first dissolved separately in a low volume of distilled water and then they were mixed together. The solution was subsequently heated at 80 °C and 120 °C. The powder was recovered, crushed in an agate mortar to improve the mechanical mixture and then retreated at 400 °C for 24 h. The resulting powder was pressed into pellet at 155 bars and then heated at 890 °C for 48 h, leading to a final deep red color powder. LeBail refinements (full pattern matching) of the powder XRD patterns were performed with the Fullprof software (Fig. 1 and Table 1 of the additional informations file). The reliability factor R_{wp} decreased to ≈11.6%. This compound crystallizes in the monoclinic system $P2_1/m$ space group. The moderate reliability factor of the $PbFe_3O(PO_4)_3$ powder XRD pattern refinement is due to the presence of a secondary phase, which we could isolate by synthesis and the composition and crystal structure of which could be determined by single crystal XRD, namely, the langbeinite $Pb_{1.5}Fe_2(PO_4)_3$. This new phase adopts the langbeinite structure type, already found in several phosphates [6–8]. The $Pb_{1.5}Fe_2(PO_4)_3$ powder was synthesized by a co-precipitation method using $Pb(NO_3)_2$, $Fe(NO_3)_3(H_2O)_9$ and $(NH_4)_2HPO_4$ as raw materials. These materials were separately dissolved in a low volume of distilled water, then mixed together and heated at 100, 200 and 400 °C to remove residual water, ammoniac and nitrate groups. The obtained powder was then pressed into pellets and sintered at 880 °C during 48 h. By doing so it was not possible to obtain a completely pure phase, as the $PbFe_3O(PO_4)_3$ was always present as a minority phase. Finally it turned out that this compound was isolated serendipitously when we tried to grow single crystals of $PbFe_3O(PO_4)_3$ by a combination of $PbFe_2(P_2O_7)_2$ flux and Bridgman methods, as described in Ref. [2]. The quartz tube which we used in replacement of the Pt one cracked during the growth run. The resulting dark green polycrystalline bulk XRD pattern proved to match with that of the secondary phase found in the $PbFe_3O(PO_4)_3$ powder. In order to check that the three successive 2nd order phase transitions that we discovered in the $PbFe_3O(PO_4)_3$ compound [2] are not coupled to structural changes, we performed powder XRD at 300, 200, 100, 32.5, 28, 6 and 300 K again to assess the reversibility of the process. The cooling was insured by monitoring a He flux ranging from 0.5 L h^{-1} at room temperature to 2.5 L h^{-1} at low temperature. The data were collected in the Bragg-Brentano geometry with a 0.02° step at a rate of 0.24° min^{-1}.

2.2. $Pb_{1.5}Fe_2(PO_4)_3$ single crystal XRD data collection and structure determination

The preliminary X-ray diffraction investigation was performed at room temperature, using Mo $K\alpha$ radiations on a Kappa CCD (Bruker Nonius) diffractometer equipped with an Apex2 detector. ω and χ scans were used to control the crystalline quality of different samples and to determine cell parameters. A single crystal of suitable size ($400 \times 200 \times 200$ μm^3) was then selected.

Table 1
Atomic coordinates in $Pb_{1.5}Fe_2(PO_4)_3$.

Atom	Wyckoff position	Occ. factor	*x*	*y*	*z*
Pb1	4*a*	0.905	0.07236	0.07236	0.07236
Pb2	4*a*	0.607	0.1928	−0.3072	−0.1928
Fe1	4*a*		0.14534	0.35466	0.64534
Fe2	4*a*		0.08669	0.91331	0.41331
P1	12*b*		0.22937	0.3736	−0.03732
O1	12*b*		0.3016	0.24009	−0.02515
O2	12*b*		0.08772	0.34265	0.00809
O3	12*b*		0.2321	0.42619	−0.18285
O4	12*b*		0.30341	0.47043	0.05615

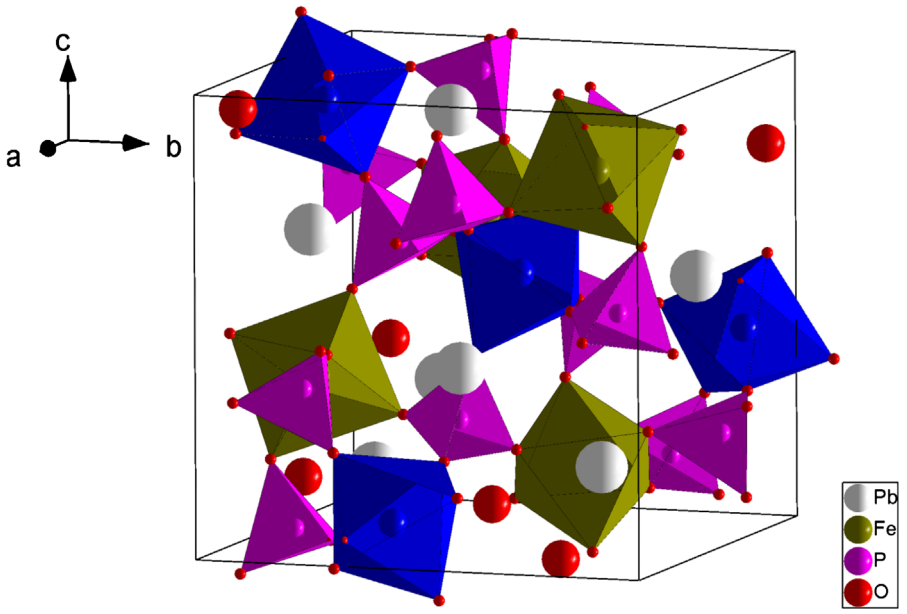

Fig.1. Drawing of the $Pb_{1.5}Fe_2(PO_4)_3$ basic unit cell which shows two crystallographically nonequivalent Fe^{3+} cations (brown and blue colors). (For interpretation of the references to color in this figure caption, the reader is referred to the web version of this article.)

A scanning angle of 0.5 ° and a Dx (detector–sample distance) value of 35 mm have been chosen; ϕ and ω scans were used. The diffracted intensities were collected up to $\theta=40°$. The diffraction pattern can be described within a cubic cell (cell parameters $a=9.7831(2)$ Å). The observed condition limiting the possible reflections, *h00: h=2n* is consistent with the space group $P2_13$. The Apex2 software suite was used to extract reflections from the collected frames and the intensities were corrected from the absorption using empirical method implemented in SADABS [9]. Details of the data collection are summarized in Table 2 of the additional informations file. A structural model considering the $P2_13$ space group has been built up with SUPERFLIP [10] using charge flipping method. Lead, iron and phosphorus atoms were located; this first model leads to a reliability factor of ~13%. It is then introduced in the refinement program Jana2006 [11]; all the atomic positions were refined, and then anisotropic displacement parameters (ADP) are considered for all the atoms. The refinement leads to an agreement factor equal to 9%. Fourier differences were then calculated allowing the location of ten oxygen atoms. The final refinement procedure leads to $R(obs)=0.045$. Atomic parameters are summarized in Tables 1 and 2 and selected interatomic distances are listed in Table 3. Large and anisotropic ADPs are observed for the oxygen atoms, which reveals a disorder that could be attributed to the existence of polyhedra tilts. This feature is illustrated in Fig. 2 of the additional informations file. Further details of the crystal structure investigations may be obtained from the Fachinformationszentrum Karlsruhe, 76344 Eggenstein-Leopoldshafen, Germany (Fax: +49 7247 808 666; e-mail: crysdata@fiz-karlsruhe.de) on quoting the depository number CSD-425066.

Table 2
Anisotropic displacement parameters in $Pb_{1.5}Fe_2(PO_4)_3$ (in Å^2).

Atom	U11	U22	U33	U12	U13	U23
Pb1	0.02711	0.02711	0.02711	−0.0007	−0.0007	−0.0007
Pb2	0.05081	0.05081	0.05081	−0.01401	0.01401	0.01401
Fe1	0.01343	0.01343	0.01343	−0.00154	0.00154	−0.00154
Fe2	0.01343	0.01343	0.01343	0.00353	0.00353	−0.00353
P1	0.00767	0.00875	0.01087	0.00155	−0.00082	−0.00332
O1	0.13863	0.06793	0.07613	0.09244	−0.03175	−0.02879
O2	0.02302	0.08522	0.0687	−0.02161	0.02359	−0.00567
O3	0.09097	0.03677	0.01801	−0.03178	−0.00739	0.00805
O4	0.08328	0.06504	0.02822	−0.05285	−0.00004	−0.02237

Table 3
Selected Pb–O distances in each Pb environment and Fe–O distances in each Fe environment in $Pb_{1.5}Fe_2(PO_4)_3$.

Pb–O distances (Å) in $Pb_{1.5}Fe_2(PO_4)_3$					
3 × Pb1	O2	2.722	3 × Pb2	O3	2.638
3 × Pb1	O1	2.938	3 × Pb2	O4	2.93
3 × Pb1	O4	2.946	3 × Pb2	O1	3.318
3 × Pb1	O1	3.255	3 × Pb2	O4	3.44
Fe–O distances (Å) in $Pb_{1.5}Fe_2(PO_4)_3$					
3 × Fe1	O3	2.009	3 × Fe2	O1	1.952
3 × Fe1	O4	1.9852	3 × Fe2	O2	1.995

2.3. Electron-probe microanalysis (EPMA) characterizations

The chemical compositions were analyzed by EPMA with a CAMECA SX-100 apparatus working at 20 kV and 20 nA with a wavelength dispersive (WDS) spectrometer. The transverse section of the pellets was investigated. The quantitative determination was performed on the basis of intensity measurements of Lα and Mα X-ray emission lines of Pb and Kα X-ray emission lines of Fe and P. The analysis was performed using metallic iron and lead, as well as an apatite as reference compounds. Oxygen content was deduced from the cationic composition to insure the charge balance. Thus, the oxidation states of the lead cations were assumed to be 2+ and the oxidation state of the iron and phosphorus cations were assumed to be 3+ and 5+, respectively. A 50×50 μm^2 mapping section was analyzed to get the elemental content spatial distribution. The range of penetration lengths in our experimental conditions typically was ~1.9–2.5 μm. The atomic content relative error for each measurement was estimated to be ~2.5%. According to powder XRD, the $Pb_{1.5}Fe_2(PO_4)_3$ minority secondary phase is present in the $PbFe_3O(PO_4)_3$ pellet, which may induce a non-stoichiometry of the majority phase, so that we decided to use as a reference the single crystal surface composition of Ref. [2], particularly uniform and of cationic composition very close to the nominal one, namely Pb 4.7 ± 0.3 at%, Fe 15.8 ± 0.4 at%, P 14.6 ± 0.4 at%. We also systematically eliminated the bad counting statistics which corresponded, in fact, to the porosities distributed over the whole surfaces investigated. By doing so, we could identify the minority secondary phase, and essentially one dominant kind of cationic non-stoichiometry in the majority phase, that is Pb 5.0–6.2 at%, Fe 13.0–14.6 at% and P 15.1–16.1 at%.

2.4. Differential scanning calorimetry (DSC)

Calorimetric measurements were performed from 295 to 1335 K at a temperature variation rate of $\beta=+5$ °C/min≈+84 mK/s for the

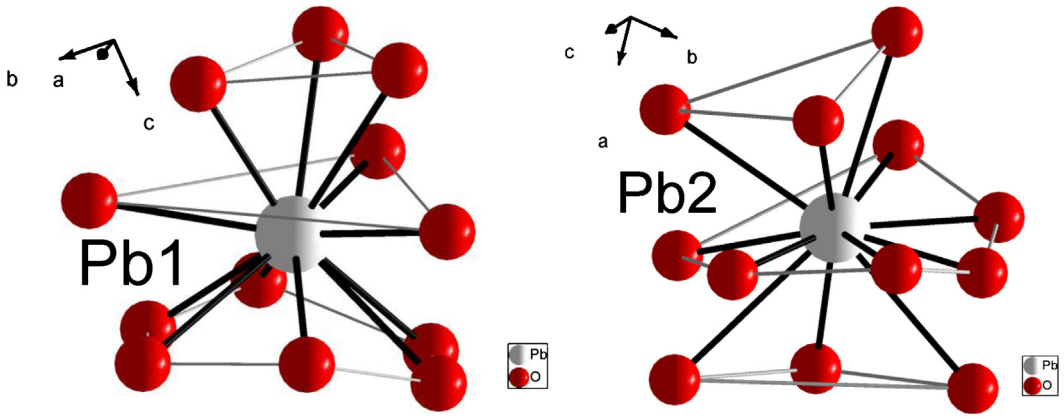

Fig. 2. The two different Pb^{2+} cations crystallographic environments in $Pb_{1.5}Fe_2(PO_4)_3$: (a) Pb1 and (b) Pb2.

heating stage and $\beta = -10$ °C/min≈−168 mK/s for the cooling stage, with a commercial continuous disk-type heat flux differential scanning calorimeter. The $PbFe_3O(PO_4)_3$ powder used ($m = 93.2$ mg) comes from a section taken from a sintered rod that was synthesized by co-precipitation. It was placed in a boron nitride (BN) crucible under Ar.

2.5. Specific heat and magnetic measurements

Magnetic susceptibility and ZFC-FC magnetization cycles were measured using a Quantum Design SQUID MPMS XL magnetometer operating in the 4.2–350 K temperature range and in the 0–5 T magnetic field range. The $PbFe_3O(PO_4)_3$ sintered pellet mass was 151.5 mg. The $PbFe_3O(PO_4)_3$ single crystals were exactly the same as those described in Ref [2]. The sample was mounted in a capsule placed in a straw and the negligibly small diamagnetic contribution of the capsule was not subtracted from our data. Specific heat measurements were made on the same 151.5 mg $PbFe_3O(PO_4)_3$ pellet, and on a 99.8 mg $Pb_{1.5}Fe_2(PO_4)_3$ pellet. The sintered sample was fixed on a sapphire sample holder with vacuum grease. The sample holder was mounted on the measurement shaft of a Quantum Design PPMS equipment interfaced to operate with a 2-τ pulse-step method corrected for the grease baseline. AC magnetic susceptibility measurements were performed in a Quantum Design PPMS instrument, under a magnetic field ranging from 500 to 1200 G with frequencies ranging from 10^{-1} to 10^3 Hz.

3. Discussion

3.1. Crystal structure and specific heat of the new langbeinite $Pb_{1.5}Fe_2(PO_4)_3$ phase

The residual impurity phase that is detected by a Bragg peak at 28.8° in the $PbFe_3O(PO_4)_3$ powder XRD patterns adopts a 3D structure with $P2_13$ space group (cubic primitive cell with a lattice parameter $a = 9.7831(2)$ Å) belonging to langbeinite structure-type (Fig. 1). In this structure, there are two kinds of Fe^{3+} cations, both located in an octahedral oxygen environment. While both have the same threefold axis symmetry element of the 4*a* Wyckoff position, they differ by the Fe–O distances (Table 3). For the Fe1 atoms, there are 3 Fe–O distances of 1.9852 Å and 3 Fe–O distances of 2.009 Å. For the Fe2 atoms, there are 3 Fe–O distances of 1.952 Å and 3 Fe–O distances of 1.995 Å. It is noticeable that $Fe(1)O_6$ and $Fe(2)O_6$ octahedra are completely isolated from each other and only connected by PO_4^{3-} groups, so that only super superexchange couplings are expected for the exchange part of the magnetic interactions in this structure. Iron octahedra and phosphate groups are connected to form a 3D skeleton that accommodates two kinds of Pb^{2+} cations, Pb1 and Pb2, which randomly occupy two positions with different occupancy factors of 90.5% and 60.7%, respectively. In $Pb_{1.5}Fe_2(PO_4)_3$, the lead ions environment consists of twelve oxygen atoms (Fig. 2) in contrast with the situation in $Pb_{1.5}V_2(PO_4)_3$, in which each Pb^{2+} environment is formed by nine oxygen atoms in spite of the fact that they have the same space group and practically the same unit cell parameter a(PbFe)= 9.7831 Å and a(PbV)= 9.7818 Å [8]. The continuous symmetry analysis [12–16], carried out with our crystallographic data, shows that the deviation from inversion symmetry of the Fe1 and Fe2 octahedra is very low, 0.16% and 0.92%, respectively, and much lower than in the V-based counterpart (Table 3 of the additional informations file). The deviation from other point symmetries is also lower than 1% in both octahedra for the C_s, C_2, C_3, C_4, C_{3v}, C_{4v}, S_2, S_4, S_6, D_2, D_3 and D_4 symmetries. The continuous shape analysis reveals that these octahedra are only 0.2% and 1% deviated from the ideal shape, which is less than the V^{3+} octahedra in $Pb_{1.5}V_2(PO_4)_3$ (0.7% and 2.1%) and even less than in the $Fe(2)O_6$ octahedron in the $PbFe_3O(PO_4)_3$ phase (vide infra and Tables S4–S6 of the Supplementary material file). This might give beginnings of an explanation for the fact that $Pb_{1.5}Fe_2(PO_4)_3$ exhibits a dark green color instead of the deep red one of $PbFe_3O(PO_4)_3$. Since both V^{3+} and Fe^{3+} cations have the same ionic radius in sixfold coordination, the lower deviation of Fe1 from inversion point symmetry and of Fe2 from perfect octahedral shape should be related to the weaker coordination (8) of lead cations in $Pb_{1.5}V_2(PO_4)_3$ than in $Pb_{1.5}Fe_2(PO_4)_3$ (12). The Jahn–Teller electronic stabilization of V^{3+} cations is very likely to contribute to the driving force for these higher distortions in the V-based compound, which in turn provide the counterbalancing elastic strain energy. According to our low temperature XRD experiments described in the experimental section, which permits to follow the 28.8° Bragg diffraction peak as a function of temperature, this phase does not seem to undergo any structural phase transition down to 6 K. In addition, the specific heat measurements performed on a sintered $Pb_{1.5}Fe_2(PO_4)_3$ pellet (Fig. 3) did not present

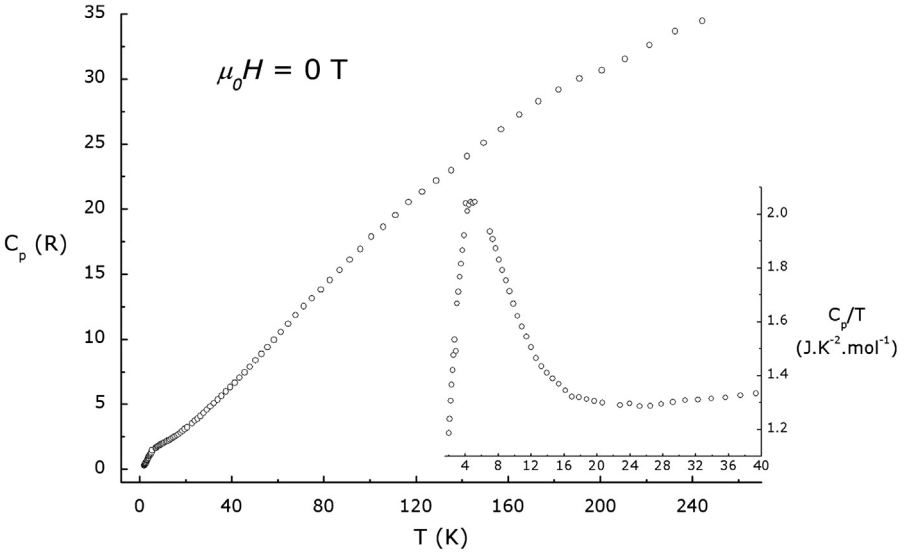

Fig. 3. $Pb_{1.5}Fe_2(PO_4)_3$ sintered pellet specific heat measurement.

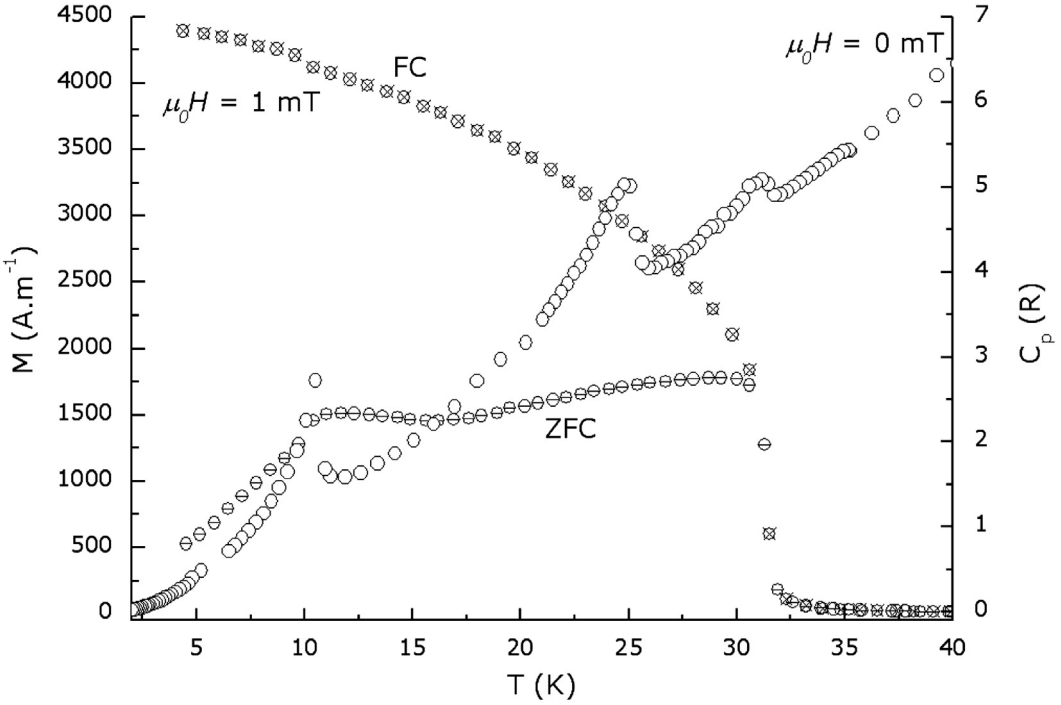

Fig. 4. Specific heat and ZFC/FC magnetization measurements of $PbFe_3O(PO_4)_3$ powder samples.

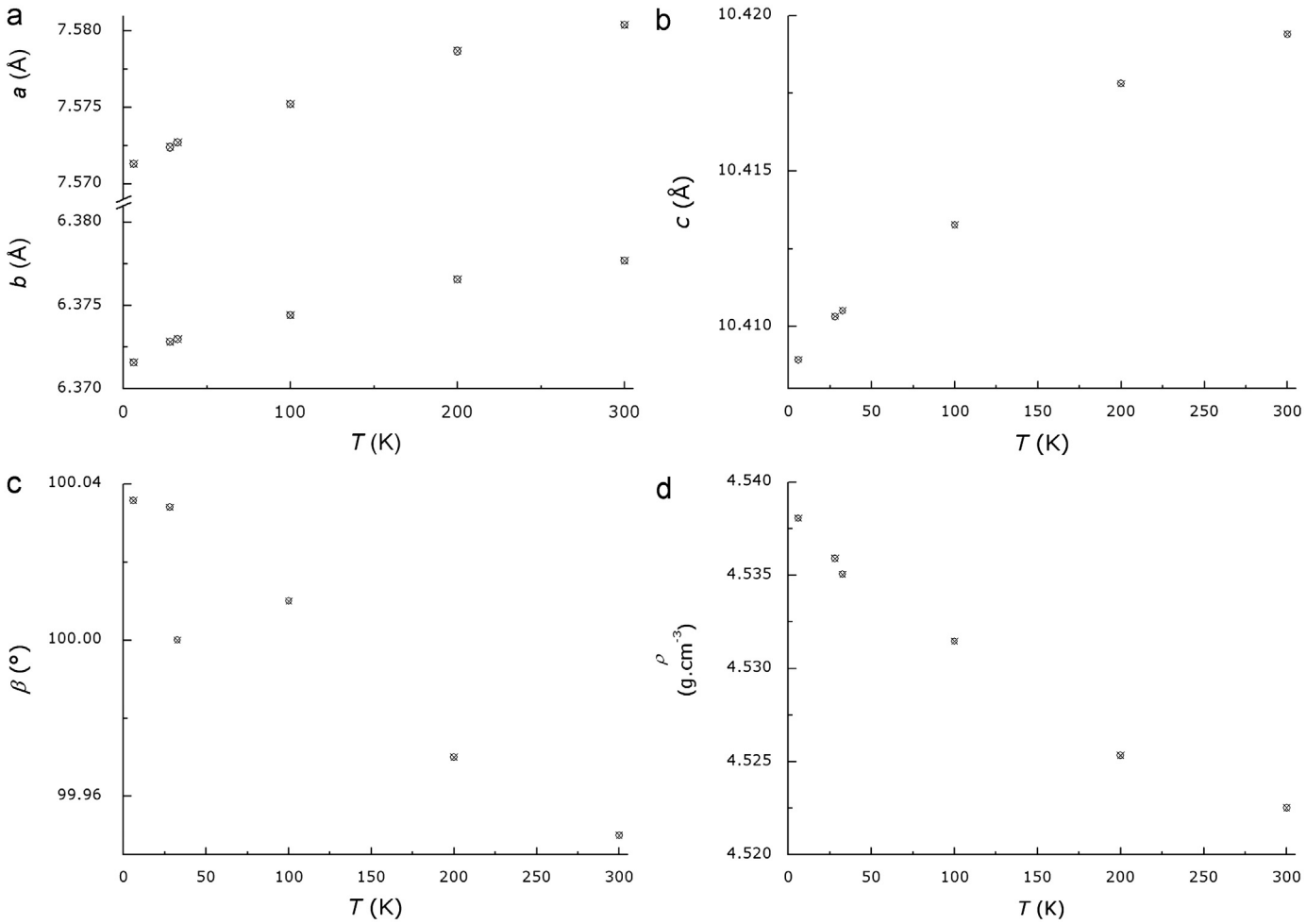

Fig. 5. (a)–(c) Thermal dependence of the $PbFe_3O(PO_4)_3$ lattice parameters; (d) thermal dependence of the $PbFe_3O(PO_4)_3$ calculated volumic mass.

any kind of divergence nor discontinuity and so there is no establishment of long range ordering in this phase down to 2 K. However, we can observe a slight cusp peaking around ~7 K which looks like a spin-glass and deserves further investigations.

3.2. Low temperature powder XRD and DSC analysis of the $PbFe_3O(PO_4)_3$ powder phase

Consequently, we can conclude that all the specific heat peaks and magnetic susceptibility divergencies observed in $PbFe_3O(PO_4)_3$ unoriented single crystals ([2]) and powders (Fig. 4) are due to the $PbFe_3O(PO_4)_3$ phase itself and do not arise from the less than 1 wt% presence of the $Pb_{1.5}Fe_2(PO_4)_3$ phase. The full profile matching refinements permit to establish the absence of any structural phase transition down to 6 K and to extract the lattice parameters thermal expansion of the $PbFe_3O(PO_4)_3$ phase. It is seen in Fig. 5 that the average density variation over the 6–300 K temperature range is rather low, ≈0.3%, as well as that of the lattice parameters, $1/a(6K)da/dT \approx 4.1 \times 10^{-6}$ K^{-1}, $1/b(6K)db/dT \approx 3.3 \times 10^{-6}$ K^{-1} and $1/c(6K)dc/dT \approx 3.4 \times 10^{-6}$ K^{-1}. Although the lattice parameters variation between 6 and 100 K looks quite linear, hence suggesting that no important change in lattice parameter thermal expansion variations takes place in this structure in the temperature range going from T_{c1} to below T_{c3}. Provided that the stability of the thermal regulation and the accuracy of the temperature measurement in our setup were sufficient, one may rule out the existence of spin–lattice couplings at play in these magnetic phase transitions. The melting onset temperature was determined to be $T_m = (1174 \pm 1)$ K, and the total latent heat and entropy corresponding to the peak observed in Fig. 6 amounts to $\Delta H = (120.6 \pm 0.9)$ kJ mol^{-1} and $\Delta S = (102.7 \pm 2.5)$ J K^{-1} mol^{-1}, respectively. However, as the solidification peak is doubled and the nucleation temperature is higher than the melting point, we suspect that this compound melts uncongruently. So, we cannot discard a small contribution of the dissolution enthalpy of some primary phase into the peritectic liquid. The macroscopic facets of the crystals arise from the smoothness of the solidification interface at the atomic level, which itself is closely related to the Jackson factor [17], defined as

$$\alpha = \frac{\Delta H_m}{RT_m} f$$

where ΔH_m denotes the melting enthalpy, T_m the melting temperature, R the ideal gas constant and f is the ratio of the number of nearest neighbor sites adjacent to an atom in the plane of the interface over the total number of nearest neighbors of this same atom in the crystal. According to the crystal structure of $PbFe_3O(PO_4)_3$, f should lie between 0.9 for (110) planes and 0.7 for (100) planes. 2D mean field theory predicts the occurrence of a surface roughening transition for a Jackson factor lower than $\alpha_C = 2$, whereas in the 2D and 3D Ising universality classes, a critical Jackson factor of 3.5 and 3.2 is found, respectively. According to our calorimetric data, if we assume that $\Delta H_m \approx \Delta H$, the material we investigated should exhibit α-values in the range 7–12, consistent with both the faceting observed and its crystallographic analysis detailed in Ref. [2].

3.3. Static and dynamic magnetic properties of the $PbFe_3O(PO_4)_3$ powders and crystals: discrepancies and extraction of critical exponents

The specific heat curve of $PbFe_3O(PO_4)_3$ sintered pellet (Fig. 4) shows three asymmetric peaks at $T_1 = 31.2$ K, $T_2 = 24.9$ K and $T_3 = 10.4$ K. While T_1 and T_3 correspond to the same transition temperatures observed in the specific heat curve of single crystals, T_2 falls in the temperature range where we observe some kind of tiny cusp in the specific heat curve of single crystals [2]. This is a striking difference between the behavior of polycrystalline sample and that of single crystals. The fact that this compound exhibits three magnetic phase transitions at low temperature, in the absence of any structural phase transition upon cooling down to 6 K, lends support to the contention that these magnetic phase transitions are due to the $PbFe_3O(PO_4)_3$ compound and not to any kind of impurity or secondary phase. The occurrence in pellets of the second peak, at T_2, is not due to the small amount of $Pb_{1.5}Fe_2(PO_4)_3$ secondary phase present in the $PbFe_3O(PO_4)_3$ pellet, because the former phase has no long range ordering down to 2 K, as was firmly established in the previous section by low temperature powder XRD as well as specific heat measurements on a $Pb_{1.5}Fe_2(PO_4)_3$ pellet. The magnetization curves show no discontinuities and two reversible FM-like phase transitions at $T_{c1} = 31.5$ K and $T_{c3} = 10.5$ K, but no such noticeable feature as that found around $T_{c2} = 23.4$ K in the single crystals curve [2]. This is another striking difference between the behavior of polycrystalline sample and that of single crystals. As these phase transitions prove to be reversible, do not seem to entail great changes in the lattice degrees of freedom (Fig. 5), and $PbFe_3O(PO_4)_3$ should remain an electronic insulator down to 2 K, they are second order magnetic phase transitions. It is probable that the second phase transition observed in sintered pellets is not a true phase transition in single crystals, but rather due to some tiny spin rotation. In previous ac magnetic susceptibility measurements [2], we noted the presence

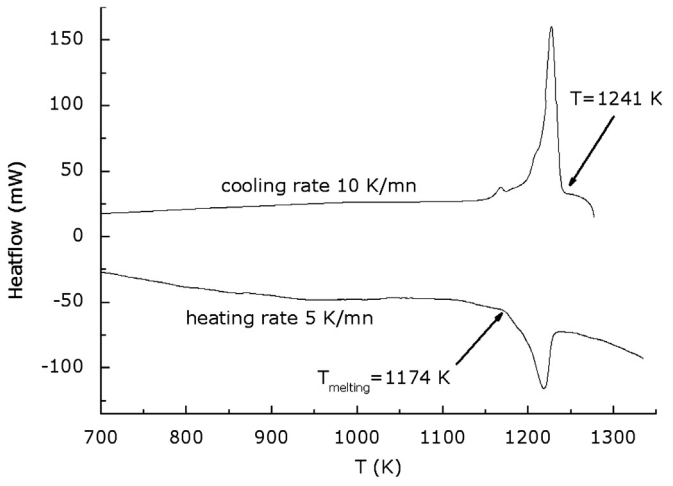

Fig. 6. DSC measurement of the $PbFe_3O(PO_4)$ powder.

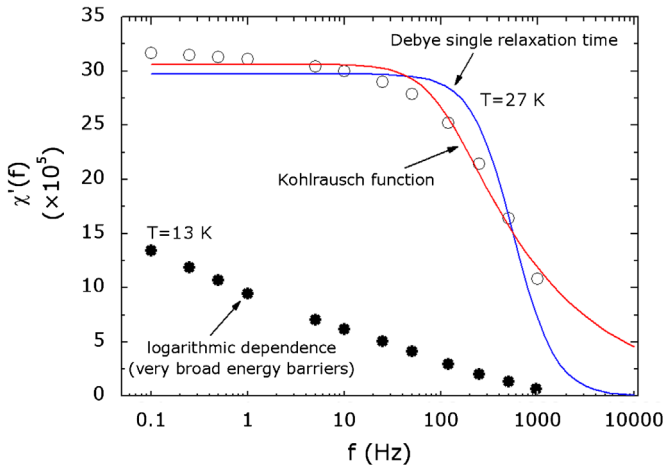

Fig. 7. AC magnetic susceptibility for different magnetic field frequencies of $PbFe_3O(PO_4)_3$ nonoriented crystals.

of two χ' and χ'' peaks around 27 and 13 K, the different frequency-dependences of which clearly proved the existence of two distinct dissipative mechanisms. Around 27 K the relaxation time almost obeys Debye-type law, or rather a Kohlrausch law (Fig. 7). The behavior around 27 K, even if it does not correspond to a perfect Debye law, still reflects a classical paramagnetic-ferromagnetic transition. At 13 K, the relaxation time distribution follows a logarithmic law which leads to a distribution of activation energies. The isothermal magnetization curve in the ordered state below T_{c3} that we reported in Ref. [2] shows two different features: (i) a fast initial increase of $M(H)$ for $\mu_0 H < 0.1$ T, indicating a large value of the susceptibility when $H \to 0$, (ii) in the field range that we could explore a slightly curved increase of $M(H)$ with a smaller slope, that makes difficult the determination of $\mu_0 H_{sat}$ by extrapolation to $M/M_{sat}=1$. We would expect $\mu_0 H_{sat} \approx k_B|\theta_p|/(gS\mu_B) \approx 53.7$ T instead of the linear extrapolation value ≈ 16.6 T. The weak FM moment M_{WF} was estimated from the intersect of the slightly curved part of $M(H)$ with $H=0$ axis. The tilt angle is given by $\sin \alpha = M_{WF}/M_{sat}$, and reaches $\alpha \sim 18.9^\circ$.

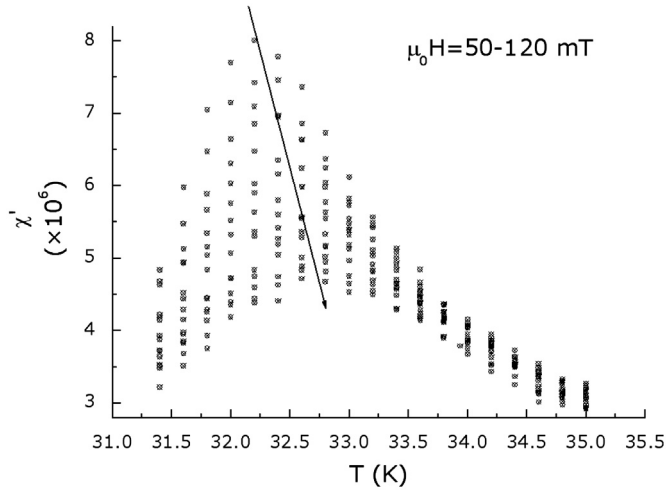

Fig. 8. AC susceptibility maxima measurements as a function of temperature, for fields from 50 mT (top) to 120 mT (bottom) of $PbFe_3O(PO_4)_3$ nonoriented crystals.

In order to extract the $PbFe_3O(PO_4)_3$ critical exponents in the vicinity of T_{c1}, we use the field- and temperature-dependence of the maximum of the ac susceptibility found in standard scaling theory [18,19] (Fig. 8): $\chi(h, t_m) \propto h^{1/\delta-1}$, $\chi(h, t_m) \propto t_m^{-\gamma}$ and $t_m \propto h^{1/(\gamma+\beta)}$ using the reduced variables $t_m=(T_M-T_c)/T_c$ and $h \sim H_i/T_c$, with T_M the location of the susceptibility maximum, $H_i=H_a-NM$ the internal field corrected for demagnetizing field effect and N being the demagnetization factor. As displayed in Fig. 9, the following values of the critical exponents were obtained: $\delta=3.03$, $\gamma=0.98$ and $\beta=0.55$. These exponents are those predicted by mean-field

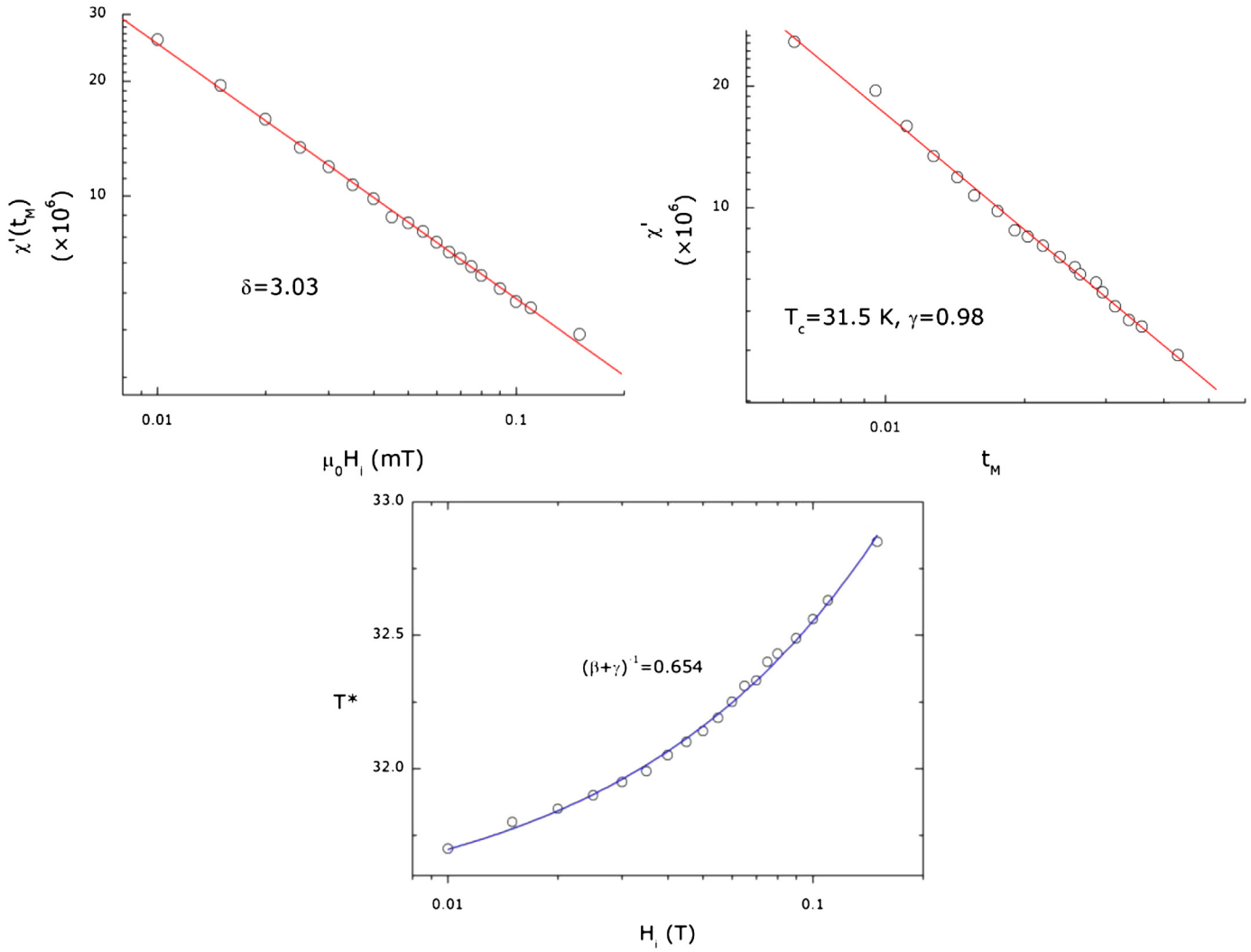

Fig. 9. The susceptibility maxima, χ_m, as a function of internal magnetic field, H_i, and as a function of the reduced temperature, t_m, of $PbFe_3O(PO_4)_3$ nonoriented crystals.

theory. This result is consistent with the fact that Arrott plots easily permit to determine $T_{c1}=31.8$ K [2], and with the corresponding specific heat peak for both single crystals and powder. Indeed, mean-field theory predicts a specific heat discontinuity at T_c, and a critical exponent $\alpha=1/2$ for temperatures lower than T_c. By subtracting a polynomial background to account for the phononic contribution, we could obtain an α value ≈ 0.6 for the temperatures lower than T_c, so that the specific heat measurements verify independently the scaling law for these three exponents. Clearly, neutron diffusion is necessary to characterize the relative variations with temperature of the AFM and the FM couplings and the effect of crystallochemical disorder, even slight, on the magnetic orderings. As a matter of fact, EPMA/WDS characterizations lead us to assume that crystallochemical disorder, likely to arise from Pb^{2+} and P^{5+} ions slight excesses together with Fe^{3+} ions depletion, is responsible for the different magnetic ZFC-FC behaviors between the sintered pellet and the single crystal, in which the FM-like second transition at T_{c2} is not seen. The presence of a small amount of the secondary phase $Pb_{1.5}Fe_2(PO_4)_3$ can give rise to crystallochemical disorder in the $PbFe_3O(PO_4)_3$ phase.

4. Conclusions

An unusual sequence of three FM-like 2nd order phase transitions in the $PbFe_3O(PO_4)_3$ oxyphosphate has been firmly established by a consistent set of room and low temperature powder XRD, specific heat, magnetization and ac/dc magnetic susceptibility measurements. A first extraction of critical exponents yielded β, δ and γ-values typical of those predicted by mean-field theory. Exploring further the $PbO–Fe_2O_3–P_2O_5$ system led to the discovery of a new langbeinite phase of chemical formula $Pb_{1.5}Fe_2(PO_4)_3$, the crystal structure of which was solved by room temperature single crystal XRD and which does not seem to undergo any structural phase transition down to 6 K nor any kind of long range ordering down to 2 K. Neutron diffusion investigations are now necessary to understand the nature of this set of FM-like transitions in $PbFe_3O(PO_4)_3$, and especially the enhancement of the 2nd C_p-peak at T_{c2} in powders as compared to single crystals.

Acknowledgments

The authors would like to thank the Aquitaine Region and the GIS “Advanced Materials in Aquitaine” for supporting this work and funding the PhD fellowship of Hassan El Hafid, as well as the French CNRS and the Morrocoan CNRST for supporting the cooperation agreement no 24494. Michel Lahaye is acknowledged for the EPMA characterization of the samples and Eric Lebraud for the low temperature powder XRD recordings.

Appendix A. Supporting information

Supplementary data associated with this article can be found in the online version at http://dx.doi.org/10.1016/j.jssc.2013.03.011.

References

[1] ICSD FindIt®, 2010.
[2] H. El Hafid, M. Velázquez, O. Pérez, A. El Jazouli, A. Pautrat, R. Decourt, P. Veber, O. Viraphong, C. Delmas., Eur. J. Inorg. Chem 36 (2011) 5486–5495. (In Fig. 4 of this article the temperature scale is to be read in Celsius degrees and not in Kelvins).
[3] E. Nakazawa, S. Shionoya, Phys. Rev. Lett. 25 (25) (1970) 1710–1712.
[4] K. Itoh, M. Madou, J. Appl. Phys. 69 (1991) 7425–7429.
[5] K. Nakatani, O. Kahn, C. Mathonière, Y. Pei, C. Zakine, J.-P. Renard, New J. Chem. 14 (1990) 861–867.
[6] R. Masse, A. Durif, J.C. Guitel, I. Tordjman, Bull. Soc. Fr. Min. Cristallogr. 95 (1972) 47.
[7] P.D. Battle, T.C. Gibb, S. Nixon, W.T.A. Harrison, J. Solid State Chem. 75 (1988) 21.
[8] R.V. Shpanchenko, O.A. Lapshina, E.V. Antipov, J. Hadermann, E.E. Kaul, C. Geibel, Mater. Res. Bull. 40 (2005) 1569–1576.
[9] G.M. Sheldrick, Sadabs Program for Scaling and Correction of Area Detector Data, Bruker AXS Inc., Madison, Wisconsin, USA, 2002.
[10] L. Palatinus, G. Chapuis, J. Appl. Cryst. *40* (2007) *786–790*.
[11] V. Petrıcek, M. Dusek L. Palatinus, The Crystallographic Computing System, Institute of Physics, Praha, Czech Republic, JANA2006, 2006.
[12] S. Alvarez, P. Alemany, D. Casanova, J. Cirera, M. Llunell, D. Avnir, Coord. Chem. Rev. 249 (2005) 1693–1708.
[13] M. Pinsky, D. Casanova, P. Alemany, S. Alvarez, D. Avnir, C. Dryzun, Z. Kizner, A. Sterkin, J. Comput. Chem. 29 (2) (2007) 190–197.
[14] S. Alvarez, D. Avnir, M. Llunell, M. Pinsky, New J. Chem. 26 (2002) 996–1009.
[15] S. Alvarez, M. Llunell, J. Chem. Soc. Dalton Trans. (2000) 3288–3303.
[16] D. Casanova, J. Cirera, M. Llunell, P. Alemany, D. Avnir, S. Alvarez, J. Am. Chem. Soc. 126 (6) (2004) 1755–1763.
[17] K.A. Jackson, in: Kinetic Processes: Crystal Growth, Diffusion, and Phase Transitions in Materials, second completely revised and enlarged edition, Wiley-VCH Verlag GmbH & Co. KGaA, Weinheim, 2010 (chapter 21).
[18] H.P. Kunkel, X.Z. Zhou, Y. Gwyn Williams, Mukovskii, D. Shulyatev, Phys. Rev B75 (2007) 012406.
[19] W. Jiang, X.Z. Zhou, G. Williams, Y. Mukovskii, K. Glazyrin, Phys. Rev. B 78 (2008) 144409.